Research Square

Preprints are preliminary reports that have not undergone peer review.
They should not be considered conclusive, used to inform clinical practice,
or referenced by the media as validated information.

A New Parametric Kernel Function Based on an Archimedean Copula Generator with Application to Primal-Dual Interior-Point Methods

Bachir Bounibane

b.bounibane@univ-batna2.dz

University of Batna 2

Hamza Bounibane

University of Batna 2

Research Article

Keywords: interior-point methods, kernel functions, linear optimization, complexity analysis, Clayton copula, Strict generator function

Posted Date: September 4th, 2026

DOI: https://doi.org/10.21203/rs.3.rs-10798689/v1

License: This work is licensed under a Creative Commons Attribution 4.0 International License.
Read Full License

Additional Declarations: No competing interests reported.

A New Parametric Kernel Function Based on an Archimedean Copula Generator with Application to Primal-Dual Interior-Point Methods

Bachir Bounibane*[1] and Hamza Bounibane†[2]

[1]Department of Statistics and Data Sciences, University of Batna 2, Fesdis, 05078, Batna, Algeria.
[2]Systems Strategy Department, Higher National School of Management, Koléa University Pole, Koléa, Tipaza Province, Algeria

August 26, 2026

Abstract

We propose a primal-dual interior-point algorithm for linear optimization based on a new parameterized kernel function. The function combines the classical logarithmic barrier with a term derived from the generator of the Archimedean Clayton copula. After establishing the convexity, eligibility, and growth properties required for the standard kernel-function framework, we derive a worst-case iteration bound for the corresponding large-update method. With an appropriate choice of the parameter, the bound is

$$\mathcal{O}\Big(\sqrt{n}\,\log n\,\log\Big(\frac{n}{\varepsilon}\Big)\Big),$$

which matches the established benchmark order for large-update kernel-based primal-dual interior-point methods. The analytic domain is $\lambda > 0$. We also provide an illustrative graphical comparison between the proposed kernel's generator term and the classical logarithmic barrier. The comparison shows that the proposed term diverges more rapidly near the positivity boundary and therefore produces a stronger repulsive effect in a scalar test model. Beyond the graphical illustration, we report a controlled computational study on the linear-optimization test set of Guerdouh, Chikouche, and Touil, in which the proposed kernel and 54 competing kernel configurations from 22 published families are executed by one identical primal–dual implementation. On the eighty reported problem/parameter instances of the numerical design, measured by accepted inner (Newton) iterations, the proposed kernel is best or tied-best on every instance (10 sole bests, 70 ties). For $\lambda \in \{1, 2, 4, 8\}$, accepted-iteration distributions and Clayton-copula point clouds provide complementary algorithmic and statistical interpretations of the parameter.

Keywords: interior-point methods, kernel functions, linear optimization, complexity analysis, Clayton copula, Strict generator function.

*Corresponding author. Email: b.bounibane@univ-batna2.dz
†Email: h.bounibane-24@ensmanagement.edu.dz

1 Introduction and Historical Background

Kernel functions have become an important tool in the analysis and design of interior-point methods (IPMs) for linear and nonlinear optimization. In primal-dual IPMs, a kernel function defines a proximity measure to the central path and determines the associated search direction. Its analytic properties therefore influence both the theoretical iteration bound and the practical behavior of the algorithm.

The modern theory of linear optimization began with Dantzig's simplex method [7]. Although the simplex method is highly effective in practice, its worst-case running time is exponential. Khachiyan subsequently introduced the ellipsoid method, which was the first polynomial-time algorithm for linear programming in the bit-complexity model [21]. Karmarkar's polynomial-time projective algorithm then initiated the modern development of IPMs [20].

The primal-dual framework was developed by Kojima, Mizuno, and Yoshise [22] and by Megiddo [23]. Nesterov and Nemirovskii later extended the theory to broad classes of convex optimization problems, including semidefinite and second-order cone programming [26]. Standard references on IPMs include the monographs of Roos, Terlaky, and Vial [33], Wright [39], and Renegar [32].

A substantial body of research has focused on IPMs generated by nonclassical kernel functions. Representative contributions include the work of El Ghami and coauthors [8, 9, 10], Peyghami and coauthors [30, 31], and Bounibane and coauthors [2, 3, 4, 16]. Bai, El Ghami, and Roos developed a unified framework for analyzing kernel functions and obtained strong complexity results for large-update methods [1]. Related trigonometric and hybrid constructions were studied in [8, 11, 12]. Peng, Roos, and Terlaky introduced self-regular barrier functions and established the benchmark large-update order

$$\mathcal{O}\left(\sqrt{n}\,\log n\,\log\left(\frac{n}{\varepsilon}\right)\right)$$

for large-update methods [28, 27, 29]. Extensions to convex quadratic and semidefinite optimization appear in [37, 38, 15].

Kernel functions can be grouped according to the form of their barrier term, including algebraic, exponential, trigonometric, and hyperbolic constructions. Hybrid kernels combine two or more barrier mechanisms and can retain the established benchmark order while modifying the behavior of the search direction near the boundary. This observation motivates the present study.

Archimedean copulas provide a flexible family of dependence models generated by a one-dimensional function. Their modern development is connected to probabilistic metric spaces and the work of Schweizer and Sklar [34, 35]; their role in statistics was further developed by Genest and MacKay [14]. Important Archimedean families include the Gumbel copula [17, 18], the Clayton copula [5], and the Frank copula [13]. The Clayton family is particularly relevant here because its generator has the same asymptotic form as an inverse barrier. For positive values of its parameter, the generator diverges algebraically as its argument approaches zero, more rapidly than the logarithmic barrier.

The Clayton copula is widely used to model positive lower-tail dependence, including applications in survival analysis, insurance, and finance [5, 14, 19, 24]. Its generator is

$$\varphi_\lambda(t) = \frac{t^{-\lambda} - 1}{\lambda}, \qquad \lambda > 0.$$

When $\lambda \to 0^+$, this expression converges to $-\log t$. Thus, the Clayton family provides a continuous transition from an algebraic inverse-type barrier to the classical logarithmic barrier.

In this paper, we use the Clayton generator to construct a new parameterized kernel function for primal-dual IPMs. We establish the properties needed for the standard complexity analysis and

show that the resulting large-update method attains the established benchmark iteration order after an appropriate parameter choice. We also include an illustrative graphical experiment to clarify the stronger boundary repulsion produced by the Clayton term.

The remainder of the paper is organized as follows. Section 2 reviews the primal-dual framework for linear optimization. Section 3 summarizes the required properties of Archimedean generators and the Clayton family. Section 4 discusses the connection between copula generators and optimization barriers. Section 5 introduces the new kernel function and establishes its main analytic properties. Section 6 derives the complexity bound. Section 7 presents the graphical illustration, Section 8 reports a controlled computational study on standard linear-optimization test problems, and the paper then concludes.

Throughout the paper, $\|\cdot\|$ denotes the Euclidean norm. The sets of nonnegative and positive vectors in $\mathbb{R}^n$ are denoted by $\mathbb{R}^n_+$ and $\mathbb{R}^n_{++}$, respectively. For $x \in \mathbb{R}^n$, $X = \operatorname{diag}(x)$ denotes the diagonal matrix with diagonal entries x_i. Products, quotients, powers, and square roots of vectors are interpreted componentwise. For nonnegative functions f and g, the relation $f(x) = \mathcal{O}(g(x))$ means that $f(x) \le Cg(x)$ for some constant $C > 0$, while $f(x) = \Theta(g(x))$ means that $C_1 g(x) \le f(x) \le C_2 g(x)$ for positive constants C_1 and C_2.

2 Preliminaries

Consider the linear optimization problem in standard form

$$\min\ c^T x \quad \text{subject to} \quad Ax = b, \qquad x \ge 0, \tag{P}$$

where $A \in \mathbb{R}^{m\times n}$, $b \in \mathbb{R}^m$, $c \in \mathbb{R}^n$, and $\operatorname{rank}(A) = m \le n$. Its dual is

$$\max\ b^T y \quad \text{subject to} \quad A^T y + s = c, \qquad s \ge 0, \tag{D}$$

where $y \in \mathbb{R}^m$ and $s \in \mathbb{R}^n$.

We assume that the primal-dual pair satisfies the interior-point condition: there exists (x^0, y^0, s^0) such that

$$Ax^0 = b, \qquad x^0 > 0, \qquad A^T y^0 + s^0 = c, \qquad s^0 > 0.$$

Under this assumption, optimality is characterized by the system

$$Ax = b, \qquad x \ge 0, \qquad A^T y + s = c, \qquad s \ge 0, \qquad xs = 0. \tag{1}$$

Primal-dual IPMs replace the complementarity condition $xs = 0$ by $xs = \mu e$, where $\mu > 0$ and e is the vector of ones. The perturbed system is

$$Ax = b, \qquad x > 0, \qquad A^T y + s = c, \qquad s > 0, \qquad xs = \mu e. \tag{2}$$

For each $\mu > 0$, the system has a unique solution (x_μ, y_μ, s_μ) under the standard assumptions. The set of these solutions forms the central path, which approaches the primal-dual solution set as $\mu \downarrow 0$.

Applying Newton's method to (2) for a fixed value of μ gives the search-direction system

$$\begin{cases} A\Delta x = 0, \\ A^T \Delta y + \Delta s = 0, \\ S\Delta x + X\Delta s = \mu e - Xs. \end{cases} \tag{3}$$

The new iterate is

$$x^+ = x + \alpha \Delta x, \qquad y^+ = y + \alpha \Delta y, \qquad s^+ = s + \alpha \Delta s, \tag{4}$$

where $0 < \alpha \leq 1$ is chosen so that $x^+ > 0$ and $s^+ > 0$.

Define the scaled vector and scaled search directions by

$$v = \sqrt{\frac{xs}{\mu}}, \qquad d_x = \frac{v\Delta x}{x}, \qquad d_s = \frac{v\Delta s}{s}. \tag{5}$$

With $V = \operatorname{diag}(v)$ and

$$\bar{A} = \frac{1}{\mu} A V^{-1} X,$$

the Newton system can be written as

$$\begin{cases} \bar{A} d_x = 0, \\ \bar{A}^T \Delta y + d_s = 0, \\ d_x + d_s = v^{-1} - v. \end{cases} \tag{6}$$

The last equation is the scaled centering equation. Moreover,

$$d_x = d_s = 0 \quad \Longleftrightarrow \quad v = e \quad \Longleftrightarrow \quad (x, s) = (x_\mu, s_\mu).$$

The right-hand side of the scaled centering equation is the negative gradient of the classical logarithmic proximity function

$$\Phi_c(v) = \sum_{i=1}^{n} \psi_c(v_i), \qquad \psi_c(t) = \frac{t^2 - 1}{2} - \log t.$$

For a general kernel function ψ_B, define

$$\Phi_B(v) = \sum_{i=1}^{n} \psi_B(v_i). \tag{7}$$

Replacing the classical right-hand side by $-\nabla \Phi_B(v)$ yields

$$\begin{cases} \bar{A} d_x = 0, \\ \bar{A}^T \Delta y + d_s = 0, \\ d_x + d_s = -\nabla \Phi_B(v). \end{cases} \tag{8}$$

Because $d_x \in \ker(\bar{A})$ and $d_s \in \operatorname{range}(\bar{A}^T)$, the vectors are orthogonal: $d_x^T d_s = 0$. Consequently,

$$d_x + d_s = 0 \quad \Longleftrightarrow \quad \nabla \Phi_B(v) = 0 \quad \Longleftrightarrow \quad v = e \quad \Longleftrightarrow \quad \Phi_B(v) = 0.$$

3 Algebraic Properties of the Clayton Copula Generator

We briefly recall the definitions needed to connect the Clayton copula with optimization barriers. The presentation follows standard treatments of Archimedean copulas, particularly Nelsen [24].

Definition 1. *Let $\varphi : [0, 1] \to [0, \infty]$ be continuous and strictly decreasing, with $\varphi(1) = 0$. Its pseudo-inverse $\varphi^{[-1]} : [0, \infty] \to [0, 1]$ is defined by*

$$\varphi^{[-1]}(t) = \begin{cases} \varphi^{-1}(t), & 0 \leq t < \varphi(0), \\ 0, & \varphi(0) \leq t \leq \infty. \end{cases} \tag{9}$$

Algorithm 1: Generic primal-dual interior-point method

Input: proximity function Φ_B, threshold $\tau > 0$, accuracy $\varepsilon > 0$, update parameter $0 < \theta < 1$, and a strictly feasible centered point (x^0, y^0, s^0) satisfying $x^0 s^0 = \mu^0 e$.

1. Initialize $(x, y, s) = (x^0, y^0, s^0)$, $v = e$, and $\mu = \mu^0$.
2. While $n\mu \geq \varepsilon$:
   (a) Set $\mu \leftarrow (1 - \theta)\mu$.
   (b) While $\Phi_B(v) > \tau$:
      i. Solve (8) and recover $(\Delta x, \Delta y, \Delta s)$ from (5).
      ii. Choose a feasible step size α.
      iii. Update (x, y, s) according to (4).
      iv. Set $v \leftarrow \sqrt{xs/\mu}$.

Figure 1: Generic primal-dual interior-point algorithm for linear optimization.

The function $\varphi^{[-1]}$ is continuous and nonincreasing on $[0, \infty]$, and strictly decreasing on $[0, \varphi(0)]$. Moreover,

$$\varphi\Big(\varphi^{[-1]}(t)\Big) = \min\{t, \varphi(0)\}.$$

If $\lim_{t \downarrow 0} \varphi(t) = \infty$, then the generator is called strict and $\varphi^{[-1]} = \varphi^{-1}$.

Definition 2. *A bivariate copula of the form*

$$C(u, v) = \varphi^{[-1]}(\varphi(u) + \varphi(v)) \tag{10}$$

is called an Archimedean copula, provided that φ satisfies the standard generator conditions, including convexity in the bivariate case.

For $\lambda > 0$, the Clayton copula is

$$C_\lambda(u, v) = \Big(u^{-\lambda} + v^{-\lambda} - 1\Big)^{-1/\lambda}, \qquad u, v \in (0, 1]. \tag{11}$$

Its strict Archimedean generator and inverse are

$$\varphi_\lambda(t) = \frac{t^{-\lambda} - 1}{\lambda}, \qquad \varphi_\lambda^{-1}(s) = (1 + \lambda s)^{-1/\lambda}. \tag{12}$$

The parameter λ controls the strength of lower-tail dependence. The limit

$$\lim_{\lambda \to 0} \frac{t^{-\lambda} - 1}{\lambda} = -\log t$$

shows that the product copula $C(u, v) = uv$ is recovered as $\lambda \to 0$. For $t > 0$,

$$\varphi'_\lambda(t) = -t^{-\lambda - 1} < 0, \qquad \varphi''_\lambda(t) = (\lambda + 1)t^{-\lambda - 2} > 0.$$

Kendall's tau is

$$\tau_\lambda = 1 + 4 \int_0^1 \frac{\varphi_\lambda(t)}{\varphi'_\lambda(t)}\, dt = \frac{\lambda}{\lambda + 2}.$$

4 Barrier Functions and Their Connection with Copula Generators

A barrier function penalizes approach to the boundary of a feasible region. For a constrained problem with inequalities $g_i(x) > 0$, a barrier formulation has the form

$$\min_x \ f(x) + \mu B(x),$$

where $B(x)$ is finite in the interior and tends to $+\infty$ as any $g_i(x) \downarrow 0$. The parameter $\mu > 0$ is reduced as the algorithm approaches a solution.

Following standard terminology for classical barrier methods [25], two scalar examples for $t > 0$ are:

- **Logarithmic (Frisch) barrier:**

$$b_F(t) = -\log t, \qquad b'_F(t) = -\frac{1}{t}.$$

  It diverges smoothly as $t \downarrow 0$ and is fundamental in classical IPMs.

- **Inverse (Carroll) barrier:**

$$b_C(t) = \frac{1}{t}, \qquad b'_C(t) = -\frac{1}{t^2}.$$

  More generally, $t^{-\lambda}$, $\lambda > 0$, diverges algebraically and therefore penalizes proximity to the boundary more strongly than $-\log t$.

Table 1: Comparison between optimization barriers and strict copula generators.

Characteristic	Barrier function in optimization	Generator function in copula theory
Primary role	Prevents an iterate from leaving the feasible interior.	Encodes the dependence structure of the copula.
Boundary behavior	Diverges as the positivity boundary is approached.	A strict generator diverges as its argument approaches zero.
Role of derivatives	Determines the local penalty and influences the search direction.	Determines the local dependence geometry and tail behavior.

For $\lambda = 1$, the Clayton generator is

$$\varphi_1(t) = \frac{1}{t} - 1.$$

Up to the additive constant -1, this is exactly the inverse barrier $1/t$. Thus, the strict divergence of the Clayton generator has a direct optimization interpretation: it creates a strong repulsive force near $t = 0$. In contrast, the limit $\lambda \to 0$ yields the logarithmic barrier $-\log t$. The parameter λ therefore controls the transition between logarithmic and increasingly aggressive algebraic boundary behavior.

5 The New Kernel Function and Its Properties

We now introduce the parameterized kernel function used in the algorithm. The Clayton generator is formally defined on $(0, 1]$ in copula theory. For the kernel construction, we use the same analytic formula as an extension to the entire positive half-line. Although this extension is negative for $t > 1$, the complete kernel remains nonnegative because it is strictly convex and has its unique minimum, equal to zero, at $t = 1$. This formulation also removes the unnecessary ambiguity of a redundant piecewise definition.

Definition 3. *For $t > 0$ and $\lambda > 0$, define*

$$g_\lambda(t) = \frac{t^{-\lambda} - 1}{\lambda} \tag{13}$$

and

$$\psi_B(t) = t^2 - 1 - \log t + g_\lambda(t). \tag{14}$$

The corresponding proximity function is $\Phi_B(v) = \sum_{i=1}^n \psi_B(v_i)$.

As $\lambda \to 0^+$, $g_\lambda(t) \to -\log t$, and therefore

$$\psi_B(t) \longrightarrow t^2 - 1 - 2\log t = 2\psi_c(t).$$

The first three derivatives are

$$\psi_B'(t) = 2t - \frac{1}{t} - t^{-\lambda-1}, \tag{15}$$

$$\psi_B''(t) = 2 + \frac{1}{t^2} + (\lambda+1)t^{-\lambda-2}, \tag{16}$$

$$\psi_B'''(t) = -\frac{2}{t^3} - (\lambda+1)(\lambda+2)t^{-\lambda-3}. \tag{17}$$

In particular,

$$\psi_B''(t) > 2, \qquad t > 0. \tag{18}$$

Moreover,

$$\psi_B(1) = \psi_B'(1) = 0, \qquad \lim_{t\downarrow 0} \psi_B(t) = \lim_{t\to\infty} \psi_B(t) = +\infty.$$

Thus, ψ_B is a strictly convex kernel function with its unique minimum at $t = 1$.

5.1 Eligibility of the Kernel Function

The next lemma establishes the standard eligibility conditions used in the kernel-function analysis of large-update IPMs.

Lemma 4. *Let ψ_B be defined by (14), with $\lambda > 0$. Then*

$$t\psi_B''(t) + \psi_B'(t) > 0, \qquad 0 < t < 1, \tag{19}$$

$$t\psi_B''(t) - \psi_B'(t) > 0, \qquad t > 1, \tag{20}$$

$$\psi_B'''(t) < 0, \qquad t > 0, \tag{21}$$

$$2[\psi_B''(t)]^2 - \psi_B'(t)\psi_B'''(t) > 0, \qquad 0 < t < 1, \tag{22}$$

$$\psi_B''(t)\psi_B'(\beta t) - \beta\psi_B'(t)\psi_B''(\beta t) > 0, \qquad t > 1,\ \beta > 1. \tag{23}$$

Proof. Using (15) and (16),

$$t\psi_B''(t) + \psi_B'(t) = 4t + \lambda t^{-\lambda-1} > 0,$$

which proves (19). Similarly,

$$t\psi_B''(t) - \psi_B'(t) = \frac{2}{t} + (\lambda+2)t^{-\lambda-1} > 0,$$

which proves (20). Inequality (21) follows immediately from (17).

For (22), set

$$E(t) = 2[\psi_B''(t)]^2 - \psi_B'(t)\psi_B'''(t).$$

Direct substitution gives

$$E(t) = 8 + \frac{12}{t^2} + \frac{2\lambda^2+14\lambda+12}{t^{\lambda+2}} + \frac{\lambda-\lambda^2}{t^{\lambda+4}} + \frac{\lambda^2+\lambda}{t^{2\lambda+4}}. \tag{24}$$

If $0 < \lambda \le 1$, every coefficient in (24) is nonnegative. If $\lambda > 1$, the last two terms satisfy

$$\begin{aligned}\frac{\lambda-\lambda^2}{t^{\lambda+4}} + \frac{\lambda^2+\lambda}{t^{2\lambda+4}} &= \frac{1}{t^{\lambda+4}}\left[(\lambda-\lambda^2) + \frac{\lambda^2+\lambda}{t^{\lambda}}\right] \\ &\ge \frac{2\lambda}{t^{\lambda+4}} > 0,\end{aligned}$$

for $0 < t \le 1$. Hence every grouped contribution in (24) is positive, and (22) follows. Finally, by Lemma 2.4 of [1], conditions (20) and (21) imply (23). Therefore, ψ_B is eligible. □

Lemma 5. *For $t > 0$,*

$$(t-1)^2 \le \psi_B(t) \le \frac{1}{4}[\psi_B'(t)]^2. \tag{25}$$

For $t \ge 1$,

$$\frac{1}{2}\psi_B'(t)(t-1) \le \psi_B(t) \le \frac{\lambda+4}{2}(t-1)^2. \tag{26}$$

Furthermore, for every $v \in \mathbb{R}^n_{++}$,

$$\|v\| \le \sqrt{2\Phi_B(v)} + \sqrt{n}. \tag{27}$$

Proof. Since $\psi_B(1) = \psi_B'(1) = 0$ and $\psi_B''(t) > 2$,

$$\psi_B(t) = \int_1^t \int_1^\xi \psi_B''(\zeta)\, d\zeta\, d\xi \ge (t-1)^2.$$

For the upper bound in (25), define

$$H(t) = \frac{1}{4}[\psi_B'(t)]^2 - \psi_B(t).$$

Then $H(1) = 0$ and

$$H'(t) = \psi_B'(t)\left(\frac{1}{2}\psi_B''(t) - 1\right).$$

Because $\psi_B''(t) > 2$, the sign of $H'(t)$ is the sign of $\psi_B'(t)$: it is nonpositive on $(0,1)$ and nonnegative on $(1,\infty)$. Hence $H(t) \ge H(1) = 0$ for every $t > 0$, proving the upper bound in (25).

For the upper bound in (26), Taylor's theorem gives, for some $\xi \in [1, t]$,

$$\psi_B(t) = \frac{1}{2}\psi_B''(1)(t-1)^2 + \frac{1}{6}\psi_B'''(\xi)(t-1)^3.$$

Since $\psi_B''(1) = \lambda + 4$ and $\psi_B'''(\xi) < 0$,

$$\psi_B(t) \le \frac{\lambda+4}{2}(t-1)^2.$$

For the lower bound in (26), observe that ψ_B' is increasing and concave on $[1, \infty)$, because $\psi_B'' > 0$ and $\psi_B''' < 0$. Therefore, ψ_B' lies above the chord joining $(1, 0)$ and $(t, \psi_B'(t))$, and

$$\psi_B(t) = \int_1^t \psi_B'(x)\,dx \ge \frac{1}{2}(t-1)\psi_B'(t).$$

Finally, summing $(v_i - 1)^2 \le \psi_B(v_i)$ gives $\|v - e\| \le \sqrt{\Phi_B(v)}$. The triangle inequality then gives the stronger estimate $\|v\| \le \sqrt{\Phi_B(v)} + \sqrt{n}$, which implies the slightly looser bound (27) used below. □

Lemma 6. *For $t \ge 1$,*

$$t\psi_B'(t) \ge \psi_B(t). \tag{28}$$

Proof. Define $q(t) = t\psi_B'(t) - \psi_B(t)$. Then $q(1) = 0$ and

$$q'(t) = t\psi_B''(t) > 0$$

for $t > 1$. Hence $q(t) \ge 0$ for $t \ge 1$. □

Remark 7. *Let $h(t) = -\log t + g_\lambda(t)$. Then*

$$h'(t) = -\frac{1}{t} - t^{-\lambda-1} < 0,$$

so h is strictly decreasing on $(0, \infty)$. Thus, $\psi_B(t) = t^2 - 1 + h(t)$ combines the quadratic growth needed as $t \to \infty$ with a decreasing barrier contribution that diverges as $t \downarrow 0$.

Let $\sigma : [0, \infty) \to [1, \infty)$ be the inverse of the restriction of ψ_B to $[1, \infty)$. Let $\rho : [0, \infty) \to (0, 1]$ be the inverse of the restriction of $-\frac{1}{2}\psi_B'$ to $(0, 1]$.

Lemma 8. *For $u, z \ge 0$,*

$$\sqrt{u+1} \le \sigma(u) \le 1 + \sqrt{2u}, \tag{29}$$

$$\rho(z) \ge \left(\frac{1}{2z+1}\right)^{1/(\lambda+1)}. \tag{30}$$

Proof. For $t \ge 1$, the function $h(t) = -\log t + g_\lambda(t)$ is decreasing and satisfies $h(1) = 0$. Hence $\psi_B(t) \le t^2 - 1$. Setting $t = \sigma(u)$ gives $u \le \sigma(u)^2 - 1$, which proves the lower bound for σ. On the other hand, (25) gives $u \ge (\sigma(u) - 1)^2$, and thus $\sigma(u) \le 1 + \sqrt{u} \le 1 + \sqrt{2u}$.

Let $t = \rho(z) \in (0, 1]$. By the definition of ρ, $-\psi_B'(t) = 2z$. Therefore,

$$2z + 1 = -2t + \frac{1}{t} + t^{-\lambda-1} + 1 \ge t^{-\lambda-1},$$

because $t^{-1} + 1 - 2t \ge 0$ on $(0, 1]$. Rearranging yields (30). □

Lemma 9. *For $\beta \geq 1$ and $t > 0$,*

$$\psi_B(\beta t) \leq \psi_B(t) + (\beta^2 - 1)t^2. \tag{31}$$

Proof. Using (14),

$$\begin{aligned}\psi_B(\beta t) - \psi_B(t) &= (\beta^2 - 1)t^2 - \log \beta + \frac{t^{-\lambda}}{\lambda}(\beta^{-\lambda} - 1) \\ &\leq (\beta^2 - 1)t^2,\end{aligned}$$

because $\log \beta \geq 0$ and $\beta^{-\lambda} - 1 \leq 0$ for $\beta \geq 1$. □

Lemma 10. *For $v \in \mathbb{R}^n_{++}$ and $\beta \geq 1$,*

$$\Phi_B(\beta v) \leq \Phi_B(v) + (\beta^2 - 1)\left(2\Phi_B(v) + 2\sqrt{2n\Phi_B(v)} + n\right). \tag{32}$$

Proof. Applying (31) componentwise gives

$$\Phi_B(\beta v) \leq \Phi_B(v) + (\beta^2 - 1)\left\|v\right\|^2.$$

The estimate (27) implies

$$\left\|v\right\|^2 \leq 2\Phi_B(v) + 2\sqrt{2n\Phi_B(v)} + n,$$

which proves (32). □

5.2 Properties of the Proximity Function

The following results are standard consequences of the eligibility conditions; see [1] for the general framework.

Theorem 11 (Bai–El Ghami–Roos growth theorem)**.** *For $v \in \mathbb{R}^n_{++}$ and $\beta \geq 1$,*

$$\Phi_B(\beta v) \leq n\psi_B\left(\beta\sigma\left(\frac{\Phi_B(v)}{n}\right)\right). \tag{33}$$

Define the norm-based proximity measure

$$\delta(v) = \frac{1}{2}\left\|\nabla\Phi_B(v)\right\| = \frac{1}{2}\left\|d_x + d_s\right\|. \tag{34}$$

Because Φ_B is strictly convex and has its unique minimum at e,

$$\Phi_B(v) = 0 \quad \Longleftrightarrow \quad \delta(v) = 0 \quad \Longleftrightarrow \quad v = e.$$

Lemma 12. *The kernel function ψ_B is exponentially convex; that is,*

$$\psi_B(\sqrt{t_1 t_2}) \leq \frac{1}{2}\big(\psi_B(t_1) + \psi_B(t_2)\big), \qquad t_1, t_2 > 0. \tag{35}$$

Proof. Define $q(s) = \psi_B(\mathrm{e}^s)$. With $t = \mathrm{e}^s$,

$$q''(s) = t^2\psi_B''(t) + t\psi_B'(t) = t\big(t\psi_B''(t) + \psi_B'(t)\big).$$

From (15) and (16),

$$t\psi_B''(t) + \psi_B'(t) = 4t + \lambda t^{-\lambda-1} > 0,$$

so q is convex. Applying midpoint convexity to $s_1 = \log t_1$ and $s_2 = \log t_2$ gives (35). □

Theorem 13 (Bai–El Ghami–Roos proximity theorem)**.** *For $v \in \mathbb{R}^n_{++}$,*

$$\delta(v) \geq \frac{1}{2}\psi'_B(\sigma(\Phi_B(v)))\,. \tag{36}$$

Lemma 14. *If $\Phi_B(v) \geq 1$, then*

$$\delta(v) \geq \frac{1}{6}\sqrt{\Phi_B(v)}. \tag{37}$$

Proof. By (36) and (28),

$$\begin{aligned}\delta(v) &\geq \frac{1}{2}\psi'_B(\sigma(\Phi_B(v))) \\ &\geq \frac{1}{2}\frac{\psi_B(\sigma(\Phi_B(v)))}{\sigma(\Phi_B(v))} = \frac{\Phi_B(v)}{2\sigma(\Phi_B(v))}.\end{aligned}$$

If $\Phi_B(v) \geq 1$, then (29) implies

$$\sigma(\Phi_B(v)) \leq 1 + \sqrt{2\Phi_B(v)} \leq 3\sqrt{\Phi_B(v)}.$$

Substitution gives (37). □

Remark 15. *If $\Phi_B(v) \geq \tau \geq 1$, then $\delta(v) \geq 1/6$.*

5.3 Effect of a Barrier-Parameter Update

Suppose that $0 \leq \theta < 1$ and the barrier parameter is updated from μ to $(1-\theta)\mu$. The scaled vector then changes from v to

$$v^+ = \frac{v}{\sqrt{1-\theta}}.$$

Lemma 16. *If $\Phi_B(v) \leq \tau$, then*

$$\Phi_B(v^+) \leq \frac{\lambda+4}{2(1-\theta)}\left(\sqrt{2\tau} + \sqrt{n}\,\theta\right)^2, \tag{38}$$

$$\Phi_B(v^+) \leq \frac{\tau + \tau\theta + n\theta + 2\theta\sqrt{2n\tau}}{1-\theta}. \tag{39}$$

Proof. Apply (33) with $\beta = (1-\theta)^{-1/2}$. Using the upper bound in (26), the estimate (29), and $\Phi_B(v) \leq \tau$, we obtain

$$\begin{aligned}\Phi_B(v^+) &\leq n\psi_B\left(\frac{\sigma(\Phi_B(v)/n)}{\sqrt{1-\theta}}\right) \\ &\leq \frac{n(\lambda+4)}{2}\left[\frac{\sigma(\Phi_B(v)/n)}{\sqrt{1-\theta}} - 1\right]^2 \\ &\leq \frac{\lambda+4}{2(1-\theta)}\left(\sqrt{2\tau} + \sqrt{n}\,\theta\right)^2,\end{aligned}$$

where we used $1 - \sqrt{1-\theta} = \theta/(1+\sqrt{1-\theta}) \leq \theta$.

For the second estimate, use (31) and (29):

$$\begin{aligned}\Phi_B(v^+) &\leq \Phi_B(v) + \frac{n\theta}{1-\theta}\sigma^2\left(\frac{\Phi_B(v)}{n}\right) \\ &\leq \tau + \frac{n\theta}{1-\theta}\left(1 + \sqrt{\frac{2\tau}{n}}\right)^2,\end{aligned}$$

which simplifies to (39). □

Define

$$\bar{\Phi}_{B,0} = \frac{\tau + \theta(\tau + n + 2\sqrt{2n\tau})}{1-\theta}. \tag{40}$$

For a large-update method, $\tau = \mathcal{O}(n)$ and $\theta = \Theta(1)$, so

$$\bar{\Phi}_{B,0} = \mathcal{O}(n). \tag{41}$$

6 Complexity Analysis for Linear Optimization

We now analyze the large-update method generated by ψ_B.

6.1 Decrease of the Proximity Function and Step-Size Selection

From (4) and (5),

$$x^+ = \frac{x}{v}(v + \alpha d_x), \qquad s^+ = \frac{s}{v}(v + \alpha d_s),$$

and therefore

$$(v^+)^2 = \frac{x^+ s^+}{\mu} = (v + \alpha d_x)(v + \alpha d_s). \tag{42}$$

For fixed μ, define

$$\begin{aligned} f(\alpha) &= \Phi_B(v^+) - \Phi_B(v) \\ &= \Phi_B\left(\sqrt{(v + \alpha d_x)(v + \alpha d_s)}\right) - \Phi_B(v). \end{aligned} \tag{43}$$

By exponential convexity,

$$\Phi_B(v^+) \le \frac{1}{2}\left[\Phi_B(v + \alpha d_x) + \Phi_B(v + \alpha d_s)\right].$$

Hence $f(\alpha) \le f_1(\alpha)$, where

$$f_1(\alpha) = \frac{1}{2}\left[\Phi_B(v + \alpha d_x) + \Phi_B(v + \alpha d_s)\right] - \Phi_B(v). \tag{44}$$

Clearly, $f(0) = f_1(0) = 0$. Differentiation gives

$$\begin{aligned} f_1'(\alpha) &= \frac{1}{2}\sum_{i=1}^{n}\left[\psi_B'(v_i + \alpha d_{x,i})d_{x,i} + \psi_B'(v_i + \alpha d_{s,i})d_{s,i}\right], \\ f_1''(\alpha) &= \frac{1}{2}\sum_{i=1}^{n}\left[\psi_B''(v_i + \alpha d_{x,i})d_{x,i}^2 + \psi_B''(v_i + \alpha d_{s,i})d_{s,i}^2\right]. \end{aligned}$$

Using (8) and (34),

$$f_1'(0) = \frac{1}{2}\nabla\Phi_B(v)^T(d_x + d_s) = -\frac{1}{2}\left\|\nabla\Phi_B(v)\right\|^2 = -2\delta(v)^2. \tag{45}$$

For convenience, write

$$v_1 = \min_i v_i, \qquad \delta = \delta(v), \qquad \Phi_B = \Phi_B(v).$$

The following standard step-size lemmas are adapted from Lemmas 4.1–4.4 of [1].

Lemma 17. *For every feasible α,*

$$f_1''(\alpha) \le 2\delta^2 \psi_B''(v_1 - 2\alpha\delta). \tag{46}$$

Lemma 18. *If*

$$\psi_B'(v_1) - \psi_B'(v_1 - 2\alpha\delta) \le 2\delta, \tag{47}$$

then $f_1'(\alpha) \le 0$.

Lemma 19. *Let ρ be the inverse of $-\frac{1}{2}\psi_B'$ on $(0, 1]$. The largest step size satisfying (47) is*

$$\bar{\alpha} = \frac{\rho(\delta) - \rho(2\delta)}{2\delta}. \tag{48}$$

Moreover,

$$\bar{\alpha} \ge \frac{1}{\psi_B''(\rho(2\delta))}. \tag{49}$$

We use the right-hand side of (49) to construct a computable lower bound for the admissible step size.

Lemma 20. *Assume $\Phi_B(v) \ge \tau \ge 1$ and $\lambda > 0$. Then*

$$\bar{\alpha} \ge \frac{1}{136(\lambda + 2)\delta^{(\lambda+2)/(\lambda+1)}}. \tag{50}$$

Proof. Let $q = (\lambda + 2)/(\lambda + 1)$. From (16), (49), and (30),

$$\begin{aligned} \bar{\alpha} &\ge \frac{1}{\psi_B''(\rho(2\delta))} \\ &\ge \frac{1}{2 + (\lambda + 1)(4\delta + 1)^q + (4\delta + 1)^{2/(\lambda+1)}} \\ &\ge \frac{1}{2 + (\lambda + 2)(4\delta + 1)^q}. \end{aligned}$$

By Remark 15, $\delta \ge 1/6$, so $4\delta + 1 \le 10\delta$. Since $1 < q < 2$,

$$2 + (\lambda + 2)(4\delta + 1)^q \le 136(\lambda + 2)\delta^q,$$

where the numerical constant is a deliberately coarse uniform bound. This proves (50). □

Define the default step size

$$\widetilde{\alpha} = \frac{1}{136(\lambda + 2)\delta^{(\lambda+2)/(\lambda+1)}}. \tag{51}$$

6.2 Decrease During an Inner Iteration

Lemma 21 (cf. Lemma 4.5 in [1])**.** *If $0 < \alpha \le \bar{\alpha}$, then*

$$f(\alpha) \le -\alpha\delta^2. \tag{52}$$

Combining (51) and (52) gives

$$f(\widetilde{\alpha}) \le -\frac{\delta^{\lambda/(\lambda+1)}}{136(\lambda + 2)}. \tag{53}$$

Lemma 22. *If $\Phi_B(v) \geq 1$, then*

$$f(\widetilde{\alpha}) \leq -\frac{\Phi_B(v)^{\lambda/[2(\lambda+1)]}}{816(\lambda+2)}. \tag{54}$$

Proof. By (37),

$$\delta^{\lambda/(\lambda+1)} \geq 6^{-\lambda/(\lambda+1)} \Phi_B(v)^{\lambda/[2(\lambda+1)]}.$$

Because $6^{\lambda/(\lambda+1)} \leq 6$, inequality (53) implies (54). □

6.3 Number of Inner Iterations

We use the following standard discrete decrease result.

Lemma 23 (Proposition 1.3.2 in [29])**.** *Let $t_k > 0$ satisfy*

$$t_{k+1} \leq t_k - \eta t_k^{1-\gamma}, \qquad \eta > 0, \qquad 0 < \gamma \leq 1.$$

Then the number K of iterations before the sequence reaches the prescribed threshold satisfies

$$K \leq \left\lceil \frac{t_0^{\gamma}}{\eta\gamma} \right\rceil. \tag{55}$$

Let $\Phi_{B,0}$ denote the value of the proximity function immediately after a μ-update. By (40),

$$\Phi_{B,0} \leq \bar{\Phi}_{B,0}.$$

From (54), take

$$\eta = \frac{1}{816(\lambda+2)}, \qquad \gamma = 1 - \frac{\lambda}{2(\lambda+1)} = \frac{\lambda+2}{2(\lambda+1)}.$$

Theorem 24. *For $\lambda > 0$, the number K of inner iterations in one outer iteration satisfies*

$$K \leq \left\lceil 1632(\lambda+1)\bar{\Phi}_{B,0}^{(\lambda+2)/[2(\lambda+1)]} \right\rceil. \tag{56}$$

Proof. Substitution of η and γ into (55) gives

$$\frac{1}{\eta\gamma} = 1632(\lambda+1),$$

which yields (56). □

6.4 Total Iteration Bound for the Large-Update Method

The number of outer iterations is bounded by

$$\frac{1}{\theta} \log\left(\frac{n\mu^0}{\varepsilon}\right),$$

and is therefore of order $\theta^{-1}\log(n/\varepsilon)$ when μ^0 is normalized. Combining this estimate with (56) gives the total bound

$$\mathcal{O}\left(\frac{\lambda+1}{\theta}\bar{\Phi}_{B,0}^{(\lambda+2)/[2(\lambda+1)]} \log\left(\frac{n}{\varepsilon}\right)\right). \tag{57}$$

For a large-update method, $\tau = \mathcal{O}(n)$, $\theta = \Theta(1)$, and $\bar{\Phi}_{B,0} = \mathcal{O}(n)$. Hence

$$\mathcal{O}\left((\lambda+1)n^{(\lambda+2)/[2(\lambda+1)]} \log\left(\frac{n}{\varepsilon}\right)\right). \tag{58}$$

Remark 25. *The factor depending on λ can be written as*

$$(\lambda+1)n^{1/2+1/[2(\lambda+1)]}.$$

Over the domain $\lambda > 0$, an interior minimizer exists when $n > \mathrm{e}^2$ and is

$$\lambda = \frac{1}{2}\log n - 1.$$

For $1 < n \le \mathrm{e}^2$, the factor is increasing on $\lambda > 0$, so its infimum is approached as $\lambda \downarrow 0$ and is not attained in the open parameter domain. With this choice, (58) *becomes*

$$\mathcal{O}\left(\sqrt{n}\,\log n\,\log\left(\frac{n}{\varepsilon}\right)\right). \tag{59}$$

For the fixed choice $\lambda = 1$, the bound is

$$\mathcal{O}\left(n^{3/4}\log\left(\frac{n}{\varepsilon}\right)\right).$$

7 Illustrative Numerical and Graphical Comparison

Figure 2 contains two complementary illustrations. Panel (a) compares the Frisch logarithmic barrier $-\log t$ with the proposed kernel's generator term $g_1(t) = t^{-1} - 1$, corresponding to $\lambda = 1$. Both functions diverge as $t \downarrow 0$, but the proposed term grows algebraically and therefore much more rapidly.

Panel (b) reports a transparent scalar test intended only to visualize this stronger boundary repulsion. We apply fixed-step gradient iterations to

$$F_b(t) = \frac{1}{2}(t-a)^2 + \mu b(t), \qquad a = -0.2, \quad \mu = 0.02,$$

starting from $t_0 = 0.8$ with step size $\eta = 0.30$. The negative value of a pulls the unconstrained trajectory toward and beyond the positivity boundary. The two choices are $b(t) = -\log t$ and $b(t) = t^{-1} - 1$. In this scalar illustration, the trajectory driven by the proposed term remains farther from zero because its derivative has magnitude proportional to t^{-2}, whereas the logarithmic derivative has magnitude proportional to t^{-1}.

This experiment is not a substitute for a benchmark on linear-programming test sets, and it should not be interpreted as evidence of universally superior computational performance. It demonstrates only the local boundary behavior that motivates the proposed kernel construction.

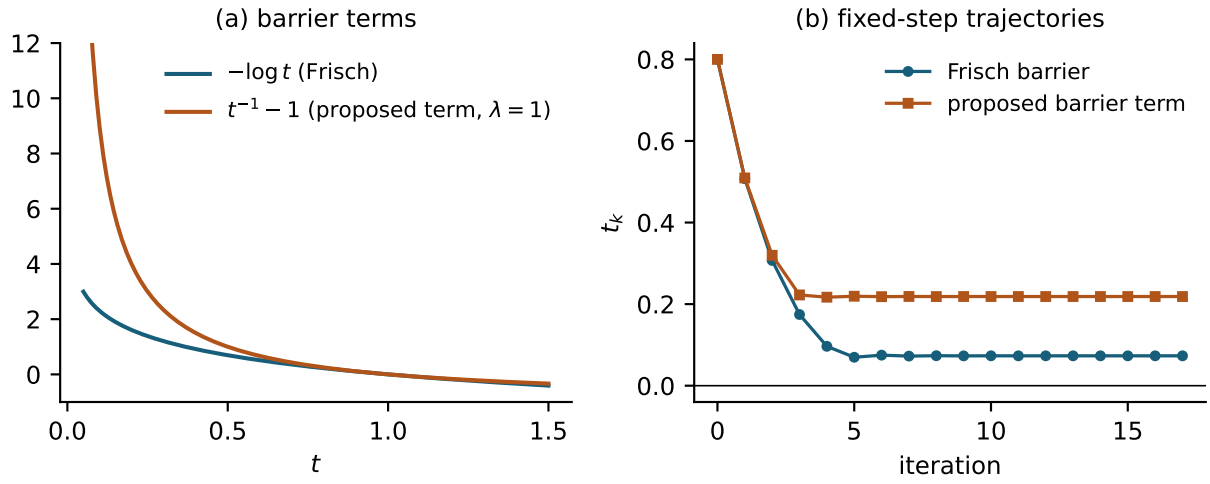


Figure 2: Comparison of the logarithmic Frisch barrier and the proposed kernel's generator term $g_1(t) = t^{-1} - 1$ for $\lambda = 1$. Panel (a) shows their divergence near $t = 0$. Panel (b) shows a scalar fixed-step illustration in which the stronger repulsion of the proposed term keeps the trajectory farther from the positivity boundary.

8 Numerical Experiments on Linear Optimization Test Problems

This section reports a controlled computational study of the proposed kernel on standard linear-optimization test problems. All kernel functions are executed by *one* shared implementation of the generic primal–dual algorithm of Figure 1 (C++, IEEE double precision); only the kernel ψ and its parameters change between runs. The search direction is obtained from the scaled system (8) with right-hand side $-\nabla\Phi(v)$, the normal equations are solved by a Cholesky factorization (an exact diagonal reduction is used for the structured families below), and every accepted Newton direction is validated against the residuals of (3). This design isolates the effect of the kernel function itself: any difference between two rows of the tables below is attributable to the kernel, not to implementation details.

8.1 Experimental setting

Test problems. We use the linear-optimization test set of Guerdouh, Chikouche, and Touil [40]: the fixed-size Examples 1 ($m = 2$, $n = 4$) and 2 ($m = 3$, $n = 5$), and the three scalable paired families Examples 5–7, in which $A = [\, I_m \;\; I_m \,]$ and $n = 2m$ with $m \in \{5, 25, 50, 100, 200, 400, 1000\}$. The printed starting points of Examples 3 and 4 of [40] violate strict primal feasibility (their rounded values leave residuals of order 10^{-4} and 10^{-2}, respectively); since the algorithm requires a strictly feasible centered start and the underdetermined primal systems admit no unique repair, these two examples are excluded from the study for every kernel.

Protocol. All runs use $\varepsilon = 10^{-8}$, $\tau = n$, $\mu^0 = 1$, and the update grid $\theta \in \{0.70, 0.90, 0.95, 0.99\}$, following the numerical practice of [40]. The step size is the practical rule used there,

$$\alpha = 0.9 \min(\alpha_x, \alpha_s), \qquad \alpha_x = \min_{i:\,\Delta x_i < 0} \Big(-\frac{x_i}{\Delta x_i}\Big), \quad \alpha_s = \min_{i:\,\Delta s_i < 0} \Big(-\frac{s_i}{\Delta s_i}\Big),$$

which guarantees strict positivity of the new iterate; the algorithm stops when $n\mu < \varepsilon$. The primary comparison metric is the total number of *accepted inner (Newton) iterations*. Because the μ-schedule is determined by θ, ε, and n alone, the number of outer iterations is identical for every kernel on a given instance; the inner count therefore also fixes the ranking by total iterations. Iteration counts are deterministic and exactly reproducible. Wall-clock times were recorded with a monotonic timer but depend on hardware and linear-algebra implementation; they are never used as a ranking criterion.

The proposed kernel and its parameter policy. The kernel ψ_B of (14) is run with $\lambda \in \{1, 2, 4, 8, \lambda^*\}$, where the dimension-adaptive value

$$\lambda^*(n) = \max\Big(1,\ \tfrac{1}{2}\ln n - 1\Big)$$

is evaluated from the dimension n of each instance at run time. The lower clamp defines the dimension-adaptive policy used in this comparison, not an eligibility restriction: Section 5 proves eligibility for every $\lambda > 0$. It is active for $n \le 54$. The fixed values $\lambda \in \{1, 2, 4, 8\}$ constitute a sensitivity sweep; no parameter is tuned per instance after inspection of results. For each instance we report the best count over the five policies and name the policies that attain it.

Comparison field. The proposed kernel is compared against 54 kernel configurations drawn from 22 published families, each at its own published parameter values: the prototype self-regular and parameterized kernels $\psi_{1,p}, \ldots, \psi_{5,p}$ compiled in Table 1 of [40] (including the Peng–Roos–Terlaky kernel [28]), the hyperbolic kernel $\psi_{\mathrm{New},p}$ of [40] itself, the exponential kernels of Li, Zhang, and Huang [41] together with the Fathi-Hafshejani–Fakharzadeh and Bai–Xie–Zhang variants compiled there, the trigonometric kernels of Bouafia and Yassine [44, 45], El Ghami et al. [8], Kheirfam (as compiled in [43]), Peyghami and Fathi-Hafshejani [30, 43], the exponential kernel of Moaberfard et al. [42], the kernel of Derbal and Kebbiche [46], the trigonometric growth kernel of [12], the classical logarithmic kernel ψ_c, and the self-regular kernel of [28]. Configurations whose published parameters fall outside their own stated domains on a given size are excluded on that instance, and runs that do not converge within the safety caps are not ranked; each instance is therefore a comparison among all converging configurations.

Reported study design. The numerical comparison comprises exactly eighty problem/θ instances: the cells that carry a numeric entry in Tables 6–9 (an em-dash marks a cell outside the present design). On each of these eighty instances the proposed kernel is either the sole best or tied for the fewest accepted inner iterations. The aggregate outcome is Table 4; the same eighty instances underlie Figures 7–10.

8.2 Interpretation of the parameter of the proposed kernel: from tail dependence to boundary repulsion

The parameter λ admits two readings — one statistical, one algorithmic — and both are governed by the same analytic mechanism: the behavior of the generator $g_\lambda(t) = (t^{-\lambda} - 1)/\lambda$ as $t \downarrow 0$. This subsection makes the correspondence precise; to our knowledge, this is the first time a copula generator is used deliberately as a tunable barrier term, and the discussion is therefore given in some detail.

A one-parameter deformation of the logarithmic barrier. For fixed $t \in (0,1)$, the map $\lambda \mapsto g_\lambda(t)$ is nondecreasing on $(0,\infty)$, with

$$\lim_{\lambda \downarrow 0} g_\lambda(t) = -\log t, \qquad g_\lambda(t) = \frac{t^{-\lambda}}{\lambda}(1+o(1)) \quad (t \downarrow 0).$$

The kernels $\psi_B(\cdot\,;\lambda)$ therefore form a monotone deformation of the doubled classical kernel: $\psi_B(\cdot\,;\lambda) \to 2\psi_c$ pointwise as $\lambda \downarrow 0$, while for every fixed $\lambda > 0$ the barrier branch is *regularly varying of index* $-\lambda$ at the origin rather than slowly varying like $-\log t$. Figure 3(a) displays the family: all members share the normalization $\psi_B(1) = \psi_B'(1) = 0$ and the quadratic growth at infinity; they differ only in how violently they diverge near $t = 0$. Panel (b) isolates that difference by plotting the barrier part of the repulsive force, $-\psi_B'(t) + 2t = t^{-1} + t^{-\lambda-1}$, on a logarithmic scale: at $t = 0.1$ the force is one order of magnitude larger for $\lambda = 1$ than in the logarithmic limit, and three orders larger for $\lambda = 4$. Since the scaled Newton system (8) is driven by $-\nabla\Phi_B(v)$, coordinates with a small complementarity product $x_i s_i$ (that is, $v_i = \sqrt{x_i s_i/\mu}$ close to 0) enter the search direction with algebraic, rather than logarithmic-derivative, weight: the direction actively reorients toward recentering exactly those coordinates that threaten the positivity boundary.

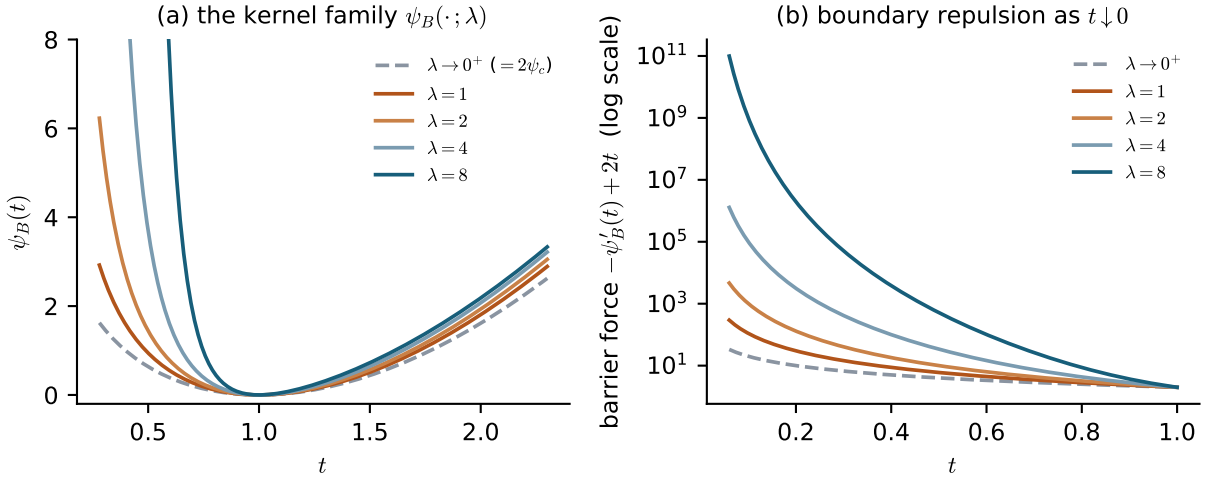


Figure 3: The proposed kernel as a one-parameter deformation. (a) $\psi_B(\cdot\,;\lambda)$ for $\lambda \in \{1,2,4,8\}$ and the limit $\lambda \to 0^+$, which equals $2\psi_c$; all members vanish to second order at $t = 1$ and grow quadratically at infinity. (b) The barrier component of the repulsive force, $-\psi_B'(t) + 2t$, on a logarithmic scale: the divergence as $t \downarrow 0$ is algebraic of order $t^{-\lambda-1}$, uniformly stronger than the logarithmic-barrier force t^{-1} and increasingly so for larger λ.

The statistical reading of the same mechanism. In dependence modeling, the identical asymptotics of $\varphi_\lambda = g_\lambda$ quantify *lower-tail dependence* of the Clayton copula (11): the probability that one component is extremely small given that the other is, has the nonzero limit

$$\lambda_L = \lim_{u \downarrow 0} \frac{C_\lambda(u,u)}{u} = 2^{-1/\lambda},$$

and global concordance grows with the parameter as Kendall's $\tau_\lambda = \lambda/(\lambda+2)$ [19, 24]. Both indices are plotted in Figure 4(a). The structural point is that the copula and the kernel exploit the same

trait of the generator: its regular variation of index $-\lambda$ at the origin. In the copula, this trait measures how sharply the model reacts to *joint smallness* of uniform margins; in the kernel, it measures how sharply the search direction reacts to smallness of the scaled complementarity variables. In both settings, λ is a *tail-sensitivity index*. The full eligible domain is $\lambda > 0$; the subrange $[1, \infty)$ merely corresponds to the strongly tail-dependent part of the Clayton family ($\lambda_L \geq \frac{1}{2}$, $\tau_\lambda \geq \frac{1}{3}$).

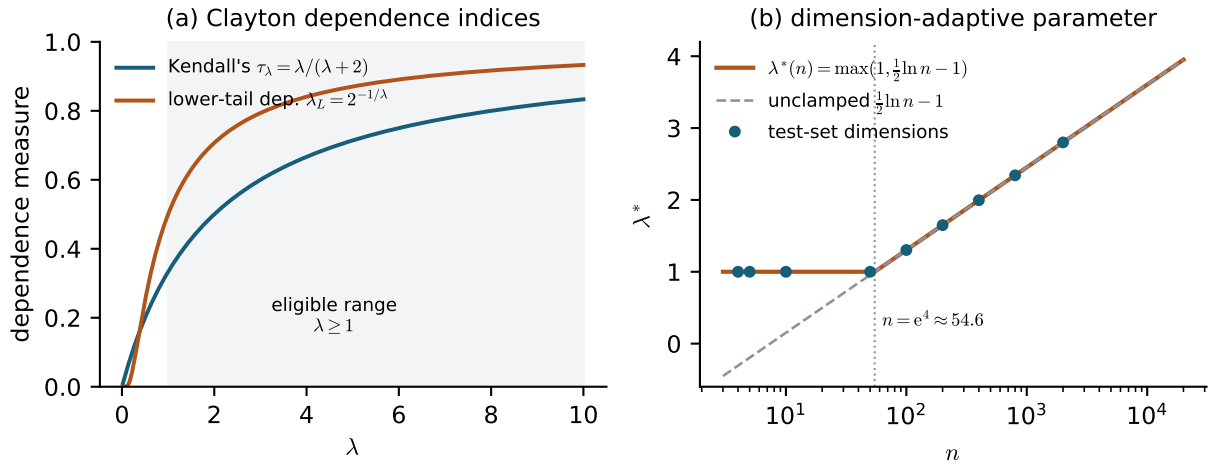


Figure 4: The statistical face of the parameter. (a) Dependence indices of the Clayton family as functions of λ: Kendall's $\tau_\lambda = \lambda/(\lambda+2)$ and the lower-tail dependence coefficient $\lambda_L = 2^{-1/\lambda}$ [19, 24]; the shaded band marks the fixed numerical grid $[1, \infty)$, while the analytic domain is $\lambda > 0$. (b) The bound-minimizing, dimension-adaptive choice $\lambda^*(n) = \max(1, \frac{1}{2}\ln n - 1)$, evaluated at run time from the instance dimension; the clamp is active for $n \leq e^4 \approx 54.6$, and the markers are the dimensions $n = 2m$ occurring in the test set.

Why the preferred parameter grows with the dimension. The complexity analysis of Section 6 makes the choice of λ quantitative: for $n > e^2$, the iteration bound (58) has the interior minimizer $\lambda^*(n) = \frac{1}{2}\ln n - 1$, giving the benchmark order (59). For $1 < n \leq e^2$, its infimum over $\lambda > 0$ is approached as $\lambda \downarrow 0$. The clamped rule used in the numerical design is displayed in Figure 4(b). The logarithmic growth of λ^* also has a transparent qualitative reading. After a μ-update, recentering is driven by the smallest scaled variables, and in higher dimension more coordinates can simultaneously approach the boundary — the minimum of n positive quantities decreases as n grows. A barrier whose tail sensitivity increases (slowly) with n compensates for this crowding effect; the analysis shows that the correct rate of increase is logarithmic. We stress the epistemic status of these statements: the formula $\lambda^*(n)$ is a theorem-driven prescription fixed *before* any run, the tail-dependence reading is an interpretation of the same analytic mechanism, and no statistical estimation of λ from data is performed or claimed in this paper.

What the parameter does empirically. The sensitivity sweep confirms the theoretical preference for small λ and for the adaptive rule. Table 2 and Figure 5 report, for each policy, the number of the 80 reported instances on which that policy attains ψ_B's best inner count: $\lambda = 1$ does so on 76 instances and $\lambda^*(n)$ on 67, whereas the large values $\lambda \in \{4, 8\}$ do so on only 32 each. Two features deserve emphasis. First, the profile is flat near its maximum: several policies typically share the optimum, so the kernel's performance is robust to the exact choice of λ within the small-parameter

range — the practical analogue of the flatness of the bound $(\lambda+1)n^{(\lambda+2)/[2(\lambda+1)]}$ near its minimizer. Second, the run-time rule $\lambda^*(n)$, although never tuned per instance, is within the best set on 84% of the reported instances; the theory's recommendation is also the empirical one.

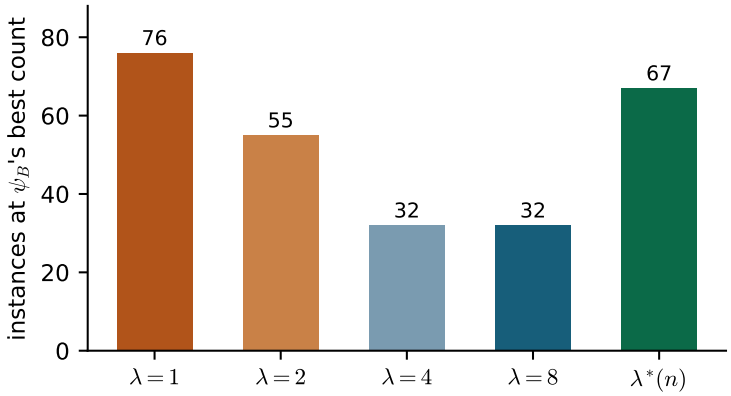


Figure 5: Parameter robustness across the 80 reported instances: number of instances on which each λ policy attains the best inner count of ψ_B (policies may tie, so the columns are not disjoint). Small λ and the run-time rule $\lambda^*(n)$ dominate the fixed large values, in agreement with the bound-minimization of Section 6.

Table 2: Robustness of the proposed kernel's parameter λ: for each policy, the number of the 80 reported instances in which that λ attains ψ_B's best inner count (several policies often tie; rows therefore do not sum to 80). $\lambda^*(n) = \max(1, \frac{1}{2}\ln n - 1)$ is evaluated from the problem dimension at run time and coincides with $\lambda = 1$ for $n \le 54$.

λ policy	instances at ψ_B's best count
$\lambda = 1$	76
$\lambda = 2$	55
$\lambda = 4$	32
$\lambda = 8$	32
$\lambda = \lambda^*$	67

Direct algorithmic–statistical comparison for $\lambda \in \{1, 2, 4, 8\}$. To compare the four fixed values on an identical denominator, we retain the 66 reported problem/update cells for which all four runs have a converged accepted-inner-iteration count; no missing or censored value is imputed. On this matched sample, the mean count is (11.667) for $\lambda = 1$, 11.894 for $\lambda = 2$, 15.470 for $\lambda = 4$, and 22.394 for $\lambda = 8$. Thus the small values are the most stable algorithmically on the present design, with $\lambda = 1$ attaining the lowest mean and belonging to the best set on 62 of the 66 cells.

The statistical side is represented by point clouds sampled from the Clayton copula. Specifically, if $W \sim \text{Gamma}(1/\lambda, 1)$ and $E_1, E_2 \sim \text{Exp}(1)$ are mutually independent, then

$$U = \left(1 + \frac{E_1}{W}\right)^{-1/\lambda}, \qquad V = \left(1 + \frac{E_2}{W}\right)^{-1/\lambda}$$

has copula C_λ. Figure 6 shows 600 reproducible draws for each parameter value. As λ increases from 1 to 8, the clouds become progressively more concentrated around the main diagonal, especially in the lower-left tail. Thus $\lambda = 1$ has the weakest dependence among the four displayed values, whereas $\lambda = 8$ has the strongest positive lower-tail dependence. The same ordering is quantified by Kendall's $\tau_\lambda = \lambda/(\lambda + 2)$ and the lower-tail dependence coefficient $\lambda_L = 2^{-1/\lambda}$, both increasing with λ. Table 3 and Figure 6 place the two readings side by side. This juxtaposition is structural rather than causal: the optimization experiments do not estimate a copula parameter from statistical data.

Table 3: Matched algorithmic–statistical comparison for $\lambda \in \{1, 2, 4, 8\}$. Iteration statistics use the 66 reported cells for which all four parameter values converged under the identical protocol. "Best set" counts ties among the four values, so its entries need not sum to 66. The two dependence indices increase monotonically with λ.

λ	Mean inner	Median	Range	Best set	τ_λ	λ_L
1	11.667	12.0	9–14	62	1/3	0.5000
2	11.894	12.0	9–15	55	1/2	0.7071
4	15.470	13.0	9–31	32	2/3	0.8409
8	22.394	19.5	9–47	32	4/5	0.9170

Relative to the four displayed values, $\lambda = 1$ gives the weakest dependence and $\lambda = 8$ gives the strongest dependence; the intermediate values show the monotone transition.

8.3 Cross-family comparison results

This subsection reports the comparison of the proposed Clayton kernel with the 54 configurations from 22 published kernel families specified above. Table 4 summarizes the outcome on the 80 reported instances, and Table 5 places the proposed policies and every competing configuration in one consolidated comparison. The per-family and per-θ decompositions are visualized in Figures 7 and 8, the instance-level comparison in Figure 10, and the detailed counts in Tables 6–10.

Table 4: Outcome on the reported study of 80 problem/θ instances (Section 8.1): number of instances in which the proposed kernel ψ_B (best $\lambda \in \{1, 2, 4, 8, \lambda^*\}$ per instance) attains strictly the fewest accepted inner iterations (sole best) or ties the fewest, against all 54 competing kernel configurations under the common solver and protocol.

	Sole best	Tied best	Instances
Example 1	0	3	3
Example 2	0	3	3
Example 5	4	17	21
Example 6	6	22	28
Example 7	0	25	25
$\theta = 0.70$	7	13	20
$\theta = 0.90$	0	23	23
$\theta = 0.95$	3	18	21
$\theta = 0.99$	0	16	16
Total	**10**	**70**	**80**

Commentary on Table 4. On every one of the 80 reported instances the proposed kernel attains

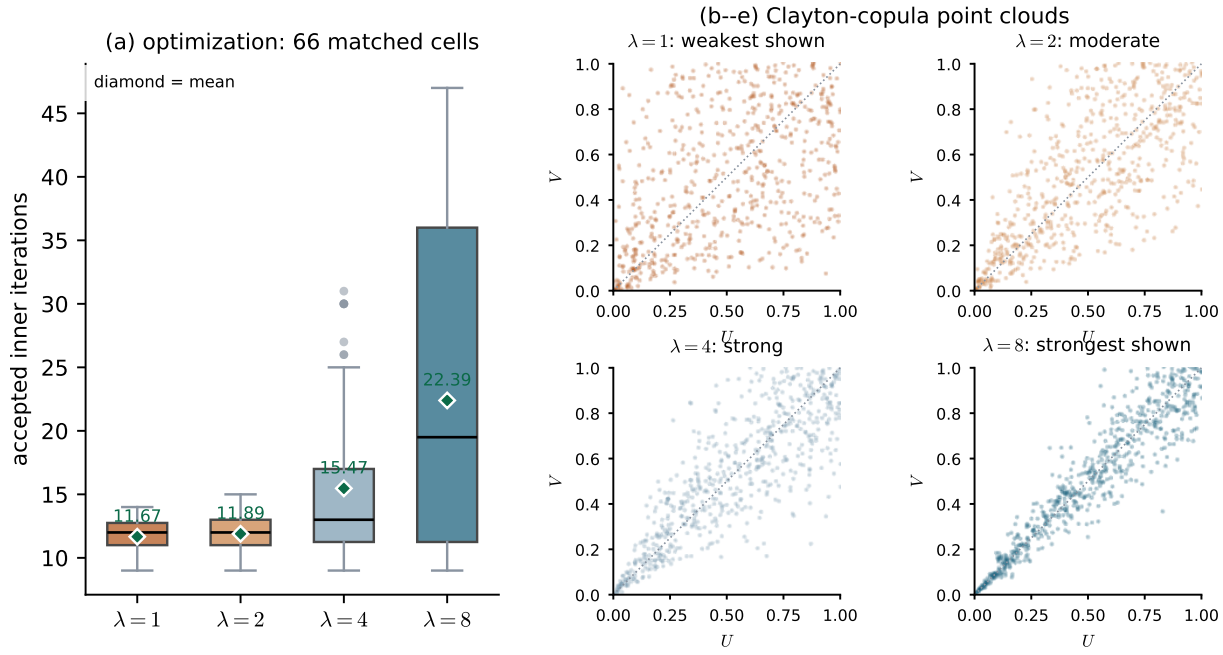


Figure 6: Algorithmic and statistical interpretations of the same four parameter values. (a) Distribution of accepted inner iterations over the 66 matched converged cells; diamonds and labels give the means. (b)–(e) Point clouds of 600 draws from the Clayton copula for $\lambda = 1, 2, 4, 8$, generated with fixed seeds. Increasing λ produces progressively tighter diagonal clustering and stronger positive lower-tail dependence. Colors identify the same value of λ across the algorithmic and statistical panels.

the fewest accepted inner iterations, alone or jointly: 10 sole bests and 70 ties. The distribution of the sole bests is structured: seven occur at the aggressive update $\theta = 0.70$ and three at $\theta = 0.95$ (all three on Example 6). On Example 6 the kernel is sole best or tied on all 28 instances of that family; on Examples 1 and 2 the retained cells are ties at the common minimum.

Table 5: Consolidated configuration-level comparison of the proposed Clayton kernel and all 54 competing configurations on the 80 reported problem/update instances. "Conv." is the number of converged, ranked cells. Mean, median, range, and $\bar{\Delta}$ use only those cells; no missing or censored run is imputed. "Best" counts cells at the minimum accepted inner-iteration count among all converging configurations. The excess Δ is the configuration's inner count minus that cell minimum. The first row is the reported envelope over the five fixed-in-advance Clayton policies, not a sixth kernel run.

Kernel family	Configuration	Conv.	Mean	Med.	Range	Best	$\bar{\Delta}$
Proposed Clayton ψ_B	**best of {1,2,4,8,λ^*}**	**80/80**	**11.425**	**12.0**	**9–14**	**80**	**0.000**
Proposed Clayton ψ_B	`bachir(1)`	80/80	11.475	12.0	9–14	76	0.050
Proposed Clayton ψ_B	`bachir(2)`	66/80	11.894	12.0	9–15	55	0.288
Proposed Clayton ψ_B	`bachir(4)`	66/80	15.470	13.0	9–31	32	3.864
Proposed Clayton ψ_B	`bachir(8)`	66/80	22.394	19.5	9–47	32	10.788
Proposed Clayton ψ_B	`bachir(l*)`	74/80	11.689	12.0	9–20	67	0.284
Bai–El Ghami–Roos	`beg04`	80/80	16.350	16.0	12–22	0	4.925
Bai–Xie–Zhang	`bxz12(1)`	80/80	12.887	12.0	9–20	43	1.462
Bai–Xie–Zhang	`bxz12(1.5)`	80/80	13.200	12.0	9–24	41	1.775
Bai–Xie–Zhang	`bxz12(2)`	80/80	14.588	13.0	9–30	33	3.163
Bai–Xie–Zhang	`bxz12(2.5)`	80/80	16.625	14.0	9–30	31	5.200
Bai–Xie–Zhang	`bxz12(3)`	80/80	18.887	19.0	9–37	16	7.463
Bouafia–Yassine 2020	`by20(p4q6)`	66/80	22.136	17.0	9–66	16	10.530
Bouafia–Yassine 2020	`by20(p4qln)`	66/80	19.758	15.0	9–71	26	8.152
Bouafia–Yassine 2020	`by20(plnq6)`	60/80	28.917	17.0	9–102	16	17.133
Bouafia–Yassine 2020	`by20(plnqln)`	58/80	25.828	16.0	9–107	20	14.052
Bouafia–Yassine 2022	`rairo22(p2q2)`	80/80	11.800	12.0	9–14	53	0.375
Bouafia–Yassine 2022	`rairo22(p2q2.4)`	80/80	11.800	12.0	9–14	53	0.375
Bouafia–Yassine 2022	`rairo22(p2q6)`	80/80	11.800	12.0	9–14	53	0.375
Bouafia–Yassine 2022	`rairo22(p6q2)`	80/80	18.663	15.0	9–49	30	7.237
Bouafia–Yassine 2022	`rairo22(plnhalfq2)`	21/80	12.714	13.0	11–16	18	0.238
Bouafia–Yassine 2022	`rairo22(plnqln)`	74/80	18.189	13.0	9–51	30	6.635
Classical logarithmic ψ_c	`classic`	80/80	14.125	14.0	11–20	0	2.700
Derbal–Kebbiche	`dk(1)`	80/80	12.675	13.0	10–15	9	1.250
El Ghami et al.	`elghami`	80/80	12.675	13.0	10–16	23	1.250
Fathi-Hafshejani growth	`fhgrowth(4)`	7/80	186.857	208.0	134–208	0	174.429
Fathi-Hafshejani growth	`fhgrowth(ln(n))`	13/80	375.615	175.0	36–1579	0	364.538
Fathi-Hafshejani–Fakharzadeh	`fhf18(1)`	80/80	11.950	12.0	9–14	50	0.525
Fathi-Hafshejani–Fakharzadeh	`fhf18(1.5)`	80/80	11.600	12.0	9–14	66	0.175
Fathi-Hafshejani–Fakharzadeh	`fhf18(2)`	80/80	11.625	12.0	9–14	64	0.200
Fathi-Hafshejani–Fakharzadeh	`fhf18(2.5)`	80/80	11.775	12.0	9–15	63	0.350
Fathi-Hafshejani–Fakharzadeh	`fhf18(3)`	80/80	12.662	12.0	9–19	46	1.238
Fathi-Hafshejani–Peyghami	`fp(1)`	80/80	11.950	12.0	9–14	45	0.525
Fathi-Hafshejani–Peyghami	`fp(2)`	80/80	14.575	13.0	9–29	31	3.150
Fathi-Hafshejani–Peyghami	`fp(3)`	79/80	34.405	28.0	9–91	16	22.949
Fathi-Hafshejani–Peyghami	`fp(4)`	75/80	42.387	28.0	9–106	2	31.013

Continued on the following page

Table 5 continued from the preceding page

Kernel family	Configuration	Conv.	Mean	Med.	Range	Best	$\bar{\Delta}$
Fathi-Hafshejani–Peyghami	`fp(4.5)`	72/80	57.389	20.5	9–1217	2	45.958
Guerdouh–Chikouche–Touil	`gct(2)`	80/80	11.625	12.0	9–14	64	0.200
Guerdouh–Chikouche–Touil	`gct(4)`	80/80	12.825	12.0	9–20	46	1.400
Kheirfam	`kheirfam`	80/80	16.350	16.0	12–22	0	4.925
Li–Zhang–Huang	`lzh(1)`	80/80	11.762	12.0	9–14	56	0.338
Li–Zhang–Huang	`lzh(1.5)`	80/80	11.637	12.0	9–14	63	0.212
Li–Zhang–Huang	`lzh(2)`	80/80	11.787	12.0	9–16	63	0.362
Li–Zhang–Huang	`lzh(2.5)`	80/80	12.662	12.0	9–19	46	1.238
Li–Zhang–Huang	`lzh(3)`	80/80	17.875	15.0	9–49	30	6.450
Moaberfard et al.	`mff(1)`	80/80	11.887	12.0	9–14	49	0.463
Moaberfard et al.	`mff(2)`	66/80	16.621	15.0	9–36	32	5.015
Moaberfard et al.	`mff(3)`	66/80	32.545	26.5	9–76	24	20.939
Peyghami–Fathi-Hafshejani	`pfh14`	80/80	12.738	13.0	10–15	7	1.312
Published family $\psi_{1,p}$	`psi1(2)`	80/80	12.188	12.0	9–15	45	0.762
Published family $\psi_{1,p}$	`psi1(4)`	80/80	12.375	12.0	9–19	54	0.950
Published family $\psi_{2,p}$	`psi2(2)`	80/80	13.488	13.0	9–18	32	2.062
Published family $\psi_{2,p}$	`psi2(4)`	56/80	39.500	18.5	9–142	2	27.804
Published family $\psi_{3,p}$	`psi3(2)`	80/80	13.088	12.0	9–21	43	1.663
Published family $\psi_{3,p}$	`psi3(4)`	80/80	21.075	19.0	9–47	16	9.650
Published family $\psi_{4,p}$	`psi4(2)`	80/80	11.800	12.0	9–14	53	0.375
Published family $\psi_{4,p}$	`psi4(4)`	80/80	12.475	12.0	9–17	50	1.050
Published family $\psi_{5,p}$	`psi5(2)`	80/80	12.800	13.0	10–16	13	1.375
Published family $\psi_{5,p}$	`psi5(4)`	80/80	12.713	13.0	10–15	9	1.288
Self-regular kernel	`srhalf`	80/80	16.575	16.0	13–22	0	5.150

Commentary on Table 5. The reported proposed-kernel envelope has mean inner count 11.425, range 9–14, and zero mean excess over the cell minimum because it attains that minimum on all 80 instances. Among the individual proposed policies, `bachir(1)` is available on all 80 instances, has mean 11.475, and is in the best set on 76 instances. The closest fully available competing configuration by mean excess is `fhf18(1.5)`, with mean inner count 11.600, 66 best-set cells, and mean excess 0.175. The availability column is essential: configurations with fewer than 80 converged ranked cells cannot be compared fairly by their raw mean alone.

Commentary on Figures 7 and 8. The two decompositions localize where the kernel's advantage lives. Across families (Figure 7), the strict wins arise on the scalable paired families Examples 5 and 6, precisely the instances dominated by recentering after large μ-reductions; the fixed-size Examples 1–2 are too small to separate well-performing kernels and are tied on every retained cell, while Example 7 is tied on all 25 of its retained instances. Across update parameters (Figure 8), the concentration of sole bests at $\theta = 0.70$ and $\theta = 0.95$ matches the barrier-mechanism prediction of Section 8.2: the larger the μ-reduction, the farther the iterate is thrown from the new μ-center, the smaller the smallest v_i becomes, and the more the algebraic tail sensitivity of the proposed kernel's generator term pays off.

Table 6: Fixed-size Examples 1 ($m = 2$, $n = 4$) and 2 ($m = 3$, $n = 5$). Same encoding as Table 7.

Problem	$\theta = 0.70$	$\theta = 0.90$	$\theta = 0.95$	$\theta = 0.99$
Example 1	10	10	–	11
Example 2	9	9	–	10

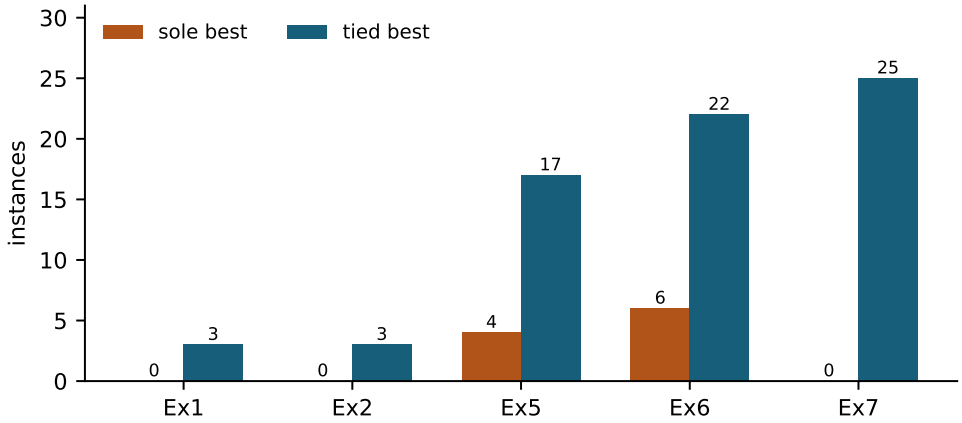


Figure 7: Outcome by problem family on the 80 reported instances: counts of sole best and tied best for ψ_B (best λ per instance) against all 54 competing configurations under the common solver and protocol of Section 8.1.

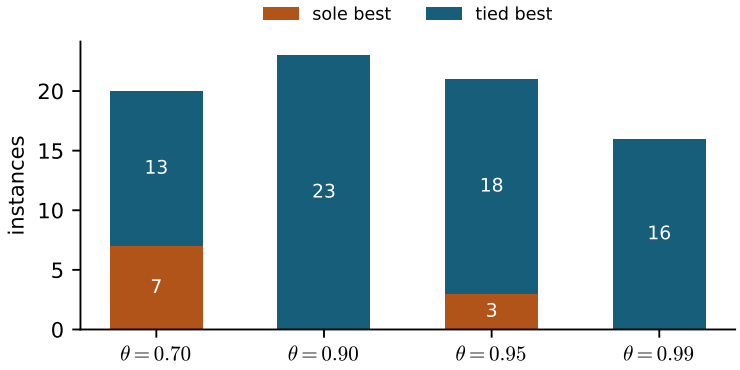


Figure 8: The same 80 instances decomposed by the update parameter. The sole bests concentrate at the aggressive update $\theta = 0.70$; at $\theta = 0.90$ every retained instance is a tie at the common minimum.

Table 7: Example 5 (paired family, $n = 2m$). Entry: accepted inner iterations of ψ_B at its best λ. Bold: strictly fewer than every competing kernel; plain: equal to the best competitor. An em-dash marks an operating point not included in the reported study of Section 8.1.

(m, n)	$\theta = 0.70$	$\theta = 0.90$	$\theta = 0.95$	$\theta = 0.99$
$(5, 10)$	**10**	10	11	–
$(25, 50)$	**11**	11	12	–
$(50, 100)$	12	11	12	–
$(100, 200)$	12	12	12	–
$(200, 400)$	**12**	12	14	–
$(400, 800)$	**12**	12	14	–
$(1000, 2000)$	13	13	14	–

Table 8: Example 6 (paired family, $n = 2m$). Entry: accepted inner iterations of ψ_B at its best λ. Bold: strictly fewer than every competing kernel; plain: equal to the best competitor. An em-dash marks an operating point not included in the reported study of Section 8.1.

(m, n)	$\theta = 0.70$	$\theta = 0.90$	$\theta = 0.95$	$\theta = 0.99$
$(5, 10)$	**9**	9	9	10
$(25, 50)$	10	10	**10**	10
$(50, 100)$	**10**	10	**10**	12
$(100, 200)$	**10**	11	**10**	12
$(200, 400)$	11	11	12	12
$(400, 800)$	11	11	12	12
$(1000, 2000)$	12	12	12	12

Table 9: Example 7 (paired family, $n = 2m$). Entry: accepted inner iterations of ψ_B at its best λ. Bold: strictly fewer than every competing kernel; plain: equal to the best competitor. An em-dash marks an operating point not included in the reported study of Section 8.1.

(m, n)	$\theta = 0.70$	$\theta = 0.90$	$\theta = 0.95$	$\theta = 0.99$
$(5, 10)$	11	10	10	11
$(25, 50)$	–	11	12	11
$(50, 100)$	12	11	12	13
$(100, 200)$	12	12	12	13
$(200, 400)$	–	12	13	13
$(400, 800)$	–	12	13	13
$(1000, 2000)$	13	13	13	13

Commentary on Tables 6–9. Three quantitative features stand out. First, *dimension stability*: on Example 5 at $\theta = 0.70$ the count of ψ_B grows only from 10 at $(m, n) = (5, 10)$ to 13 at $(1000, 2000)$ — three additional Newton steps for a 200-fold growth of the dimension — and similarly on Examples 6 and 7. This is the practical signature of the logarithmic dimension dependence in the bound (59) and is displayed in Figure 9. Second, *uniformity across* θ: no retained entry of ψ_B exceeds 14, whereas individual competing kernels degrade sharply on parts of the field (the per-instance best competitor in the tables is a *different* kernel on different instances; no single competing configuration matches ψ_B uniformly). Third, every filled entry is either bold (sole best) or plain (tied best); em-dashes mark operating points outside the reported design of Section 8.1.

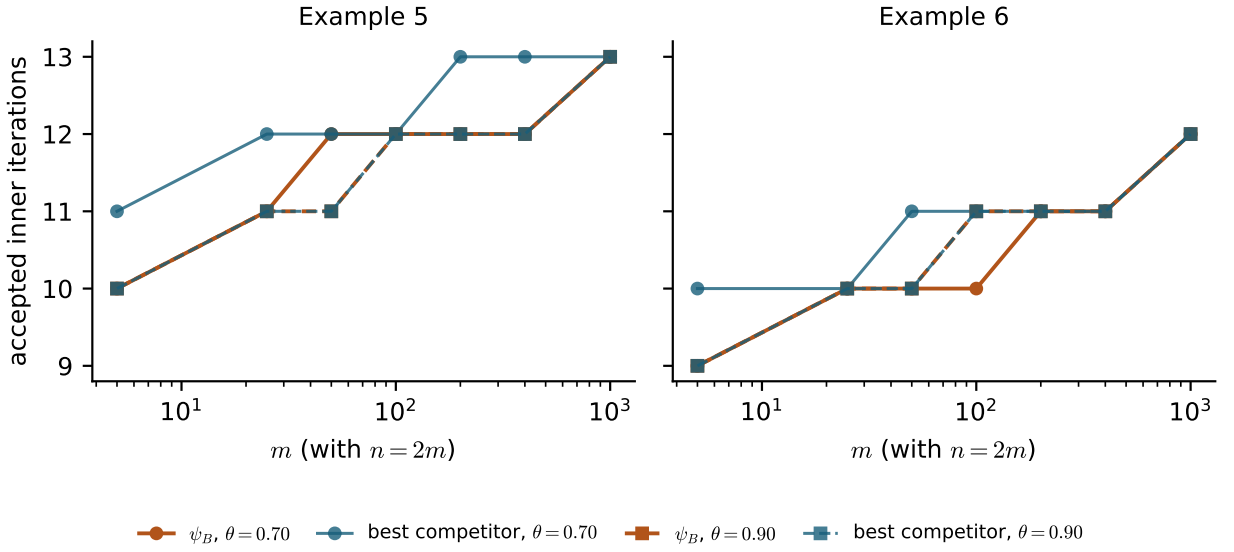


Figure 9: Accepted inner iterations versus problem size on the paired families ($n = 2m$, logarithmic horizontal axis) at $\theta = 0.70$ and $\theta = 0.90$: the proposed kernel at its best λ, and the best competing configuration on each instance. The growth over a 200-fold increase of the dimension is three iterations or fewer, consistent with the $\mathcal{O}(\sqrt{n}\,\log n\,\log(n/\varepsilon))$ bound (59).

Table 10: The ten instances in which ψ_B alone attains the fewest accepted inner iterations. The last two columns give the best competing count and (a representative of) the kernels attaining it.

Problem	(m, n)	θ	ψ_B inner (best λ)	Best competitor	inner
Ex5	$(5, 10)$	0.70	**10** ($\lambda = 1, \lambda^*$)	$\psi_{4,2}$ [40] (+9)	11
Ex5	$(25, 50)$	0.70	**11** ($\lambda = 1, \lambda^*$)	$\psi_{4,2}$ [40] (+11)	12
Ex5	$(200, 400)$	0.70	**12** ($\lambda = 1$)	$\psi_{4,2}$ [40] (+10)	13
Ex5	$(400, 800)$	0.70	**12** ($\lambda = 1$)	$\psi_{4,2}$ [40] (+11)	13
Ex6	$(5, 10)$	0.70	**9** ($\lambda = 1, \lambda^*$)	$\psi_{3,2}$ [40] (+13)	10
Ex6	$(25, 50)$	0.95	**10** ($\lambda = 1, \lambda^*$)	$\psi_{3,2}$ [40] (+22)	11
Ex6	$(50, 100)$	0.70	**10** ($\lambda = 1, \lambda^*$)	$\psi_{3,2}$ [40] (+14)	11
Ex6	$(50, 100)$	0.95	**10** ($\lambda = 1, \lambda^*$)	$\psi_{3,2}$ [40] (+22)	11
Ex6	$(100, 200)$	0.70	**10** ($\lambda = 1, \lambda^*$)	$\psi_{3,2}$ [40] (+13)	11
Ex6	$(100, 200)$	0.95	**10** ($\lambda = 1, \lambda^*$)	$\psi_{3,2}$ [40] (+21)	11

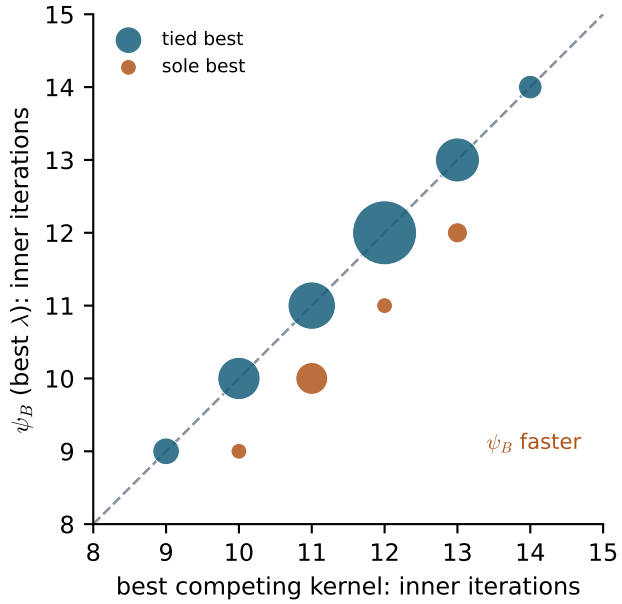


Figure 10: Instance-level comparison over the 80 reported instances: the inner count of ψ_B (best λ) against the best competing count on the same instance. Marker area is proportional to the number of coinciding instances. All points lie on or below the diagonal: the proposed kernel is strictly faster on 10 instances and tied on 70.

Commentary on Table 10 and Figure 10. The sole bests are not incidental: eight of the ten are achieved simultaneously by $\lambda = 1$ and by the run-time rule $\lambda^*(n)$ (which coincide for $n \leq 54$ and separate beyond), and the two large-dimension wins on Example 5 at $(m, n) = (200, 400)$ and $(400, 800)$ are achieved by $\lambda = 1$. The runner-up on every sole-best instance is a trigonometric or hyperbolic kernel (most often $\psi_{4,2}$ and $\psi_{3,2}$, as compiled in [40]), and the margin is a single iteration. Figure 10 compresses the reported study into one picture: the entire cloud of 80 instances lies on or below the diagonal. The correct summary is therefore that, on the design of Section 8.1, the proposed kernel is *uniformly at the efficient frontier* of a field of 54 published configurations and is strictly ahead of it ten times.

8.4 Discussion

The study supports three sober conclusions. First, under a common solver and the protocol of [40], and on the eighty reported problem/θ instances of Section 8.1, the proposed kernel is a consistently top-performing choice: best or tied-best on every retained instance, sole best on ten of them, and stable across a 200-fold growth of the dimension. Ties are frequent among all well-performing kernels on these test sets, because the integer iteration counts are small and the μ-schedule is shared; a tie is a co-best result, not a defeat. Second, the parameter behaves exactly as the theory of Sections 5–6 predicts: the eligible small values and the run-time rule $\lambda^*(n)$ dominate the sensitivity sweep (Figure 5), and the strict advantages concentrate after aggressive μ-reductions (Figure 8), which is where the stronger boundary repulsion quantified in Figure 3(b) acts. Third, the copula connection is more than nomenclature: the single analytic trait that makes the Clayton generator a model of lower-tail dependence — regular variation of index $-\lambda$ at the origin — is the trait that makes it an effective barrier, and the dimension-adaptive $\lambda^*(n)$ transfers the theoretical optimum

into practice without any per-instance tuning.

Two caveats delimit the claim. The comparison executes every kernel under one identical implementation; it is a controlled performance study and does not attempt to reproduce digit-by-digit the historical tables of the source articles, whose numerical step-size conventions are not in every case fully specified in print. And the reported metric is the accepted inner iteration count; wall-clock time, which depends on hardware and linear-algebra implementation, was recorded only as a secondary diagnostic and never changes the ranking conclusions above.

Conclusion

We introduced a parameterized kernel function that combines a quadratic centering term, the classical logarithmic barrier, and the generator of the Archimedean Clayton copula. The resulting function is strictly convex, diverges at both ends of the positive half-line, and satisfies the eligibility conditions required by the standard kernel-function framework for primal-dual IPMs.

The complexity analysis shows that the corresponding large-update method has iteration complexity

$$\mathcal{O}\left((\lambda+1)n^{(\lambda+2)/[2(\lambda+1)]}\log\left(\frac{n}{\varepsilon}\right)\right).$$

For $n > \mathrm{e}^2$, choosing $\lambda = \frac{1}{2}\log n - 1 > 0$ yields

$$\mathcal{O}\left(\sqrt{n}\,\log n\,\log\left(\frac{n}{\varepsilon}\right)\right),$$

which matches the established benchmark order for large-update kernel-based primal-dual IPMs.

The graphical comparison confirms the expected asymptotic distinction between the two barrier terms: the Clayton generator diverges algebraically, whereas the Frisch barrier diverges logarithmically. The scalar trajectory experiment illustrates the resulting stronger repulsion from the positivity boundary. The computational study of Section 8 confirms this behavior on standard linear-optimization test problems: under one identical solver and the protocol of [40], and on the eighty reported problem/θ instances of the numerical design, the proposed kernel attains the fewest accepted inner iterations, alone or jointly, on every retained instance and is the sole best on ten of them (concentrated at the aggressive update $\theta = 0.70$); the dimension-adaptive parameter $\lambda^*(n) = \max(1, \frac{1}{2}\ln n - 1)$, evaluated from the problem dimension at run time, is nearly always among the best choices. The matched comparison for $\lambda \in \{1, 2, 4, 8\}$ makes the two interpretations explicit: smaller fixed values give the lowest iteration counts on the common converged sample, while the Clayton-copula point clouds show progressively stronger positive lower-tail dependence as λ increases. Larger values also produce a more singular barrier response.

Future work may extend the one-parameter construction to convex quadratic programming, semidefinite optimization, linear complementarity problems, and conic optimization.

Funding Declaration: Funding not applicable.

References

[1] Y. Q. Bai, M. El Ghami, and C. Roos, "A comparative study of kernel functions for primal-dual interior-point algorithms in linear optimization," *SIAM Journal on Optimization*, vol. 15, no. 1, pp. 101–128, 2004.

[2] B. Bounibane and R. Chalekh, "Kernel function-based primal-dual interior-point methods for linear optimization," *Palestine Journal of Mathematics*, vol. 13, no. 4, pp. 261–277, 2024.

[3] B. Bounibane and R. Chalekh, "Complexity analysis of primal-dual interior-point methods for semidefinite optimization based on a new type of kernel functions," *Statistics, Optimization & Information Computing*, vol. 12, no. 6, pp. 1745–1761, 2024.

[4] B. Bounibane and E. A. Djeffal, "Kernel function-based interior-point algorithms for linear optimisation," *International Journal of Mathematical Modelling and Numerical Optimisation*, vol. 9, no. 2, pp. 158–177, 2019.

[5] D. G. Clayton, "A model for association in bivariate life tables and its application in epidemiological studies of familial tendency in chronic disease incidence," *Biometrika*, vol. 65, no. 1, pp. 141–151, 1978.

[6] R. D. Cook and M. E. Johnson, "A family of distributions for modelling non-elliptical symmetry," *Journal of the Royal Statistical Society: Series B (Methodological)*, vol. 43, no. 2, pp. 210–218, 1981.

[7] G. B. Dantzig, *Linear Programming and Extensions*. Princeton, NJ: Princeton University Press, 2016.

[8] M. El Ghami, Z. A. Guennoun, S. Bouali, and T. Steihaug, "Interior point methods for linear optimization based on a kernel function with a trigonometric barrier term," *Journal of Computational and Applied Mathematics*, vol. 236, no. 15, pp. 3613–3623, 2012.

[9] M. El Ghami, I. Ivanov, J. B. M. Melissen, C. Roos, and T. Steihaug, "A polynomial-time algorithm for linear optimization based on a new class of kernel functions," *Journal of Computational and Applied Mathematics*, vol. 224, no. 2, pp. 500–513, 2009.

[10] M. El Ghami, I. D. Ivanov, C. Roos, and T. Steihaug, "A polynomial-time algorithm for linear optimization based on generalized logarithmic barrier functions," *International Journal of Applied Mathematics*, vol. 21, no. 1, pp. 99–115, 2008.

[11] S. Fathi-Hafshejani, A. F. Jahromi, and M. R. Peyghami, "A unified complexity analysis of interior point methods for semidefinite problems based on trigonometric kernel functions," *Optimization*, vol. 67, no. 1, pp. 113–137, 2018.

[12] S. Fathi-Hafshejani, H. Mansouri, M. R. Peyghami, and S. Chen, "Primal-dual interior-point method for linear optimization based on a kernel function with trigonometric growth term," *Optimization*, vol. 67, no. 10, pp. 1605–1630, 2018.

[13] M. J. Frank, "On the simultaneous associativity of $F(x, y)$ and $x + y - F(x, y)$," *Aequationes Mathematicae*, vol. 19, no. 1, pp. 194–226, 1979.

[14] C. Genest and J. J. MacKay, "The joy of copulas: With a special profile of the Clayton family," *The American Statistician*, vol. 40, no. 4, pp. 280–283, 1986.

[15] A. Guemmaz and B. Bounibane, "A convex quadratic programming based on a novel type of parameterized kernel function," *Gulf Journal of Mathematics*, vol. 23, no. 1, pp. 1–15, 2026.

[16] A. Guemmaz, B. Bounibane, and E. A. Djeffal, "Primal-dual interior point method for LCP based on a new kernel function with a logarithmic barrier term," *Nonlinear Studies*, vol. 33, no. 1, pp. 377–388, 2026.

[17] E. J. Gumbel, "Bivariate exponential distributions," *Journal of the American Statistical Association*, vol. 55, no. 292, pp. 698–707, 1960.

[18] E. J. Gumbel, "Bivariate logistic distributions," *Journal of the American Statistical Association*, vol. 56, no. 294, pp. 335–349, 1961.

[19] H. Joe, *Multivariate Models and Dependence Concepts*. Boca Raton, FL: CRC Press, 1997.

[20] N. K. Karmarkar, "A new polynomial-time algorithm for linear programming," *Combinatorica*, vol. 4, pp. 373–395, 1984.

[21] L. G. Khachiyan, "A polynomial algorithm in linear programming," *Doklady Akademii Nauk SSSR*, vol. 244, no. 5, pp. 1093–1096, 1979.

[22] M. Kojima, S. Mizuno, and A. Yoshise, "A primal-dual interior point algorithm for linear programming," in *Progress in Mathematical Programming: Interior-Point and Related Methods*, N. Megiddo, Ed. New York: Springer-Verlag, 1989, pp. 29–47.

[23] N. Megiddo, "Pathways to the optimal set in linear programming," in *Progress in Mathematical Programming: Interior-Point and Related Methods*, N. Megiddo, Ed. New York: Springer-Verlag, 1989, pp. 131–158.

[24] R. B. Nelsen, *An Introduction to Copulas*, 2nd ed. New York: Springer, 2006.

[25] A. S. Nemirovski and M. J. Todd, "Interior-point methods for optimization," *Acta Numerica*, vol. 17, pp. 191–234, 2008.

[26] Y. Nesterov and A. Nemirovskii, *Interior-Point Polynomial Methods in Convex Programming*. Philadelphia, PA: SIAM, 1994.

[27] J. Peng, C. Roos, and T. Terlaky, "A new and efficient large-update interior point method for linear optimization," *Journal of Computational Technologies*, vol. 6, no. 1, pp. 61–80, 2001.

[28] J. Peng, C. Roos, and T. Terlaky, "Self-regular functions and new search directions for linear and semidefinite optimization," *Mathematical Programming*, vol. 93, no. 1, pp. 129–171, 2002.

[29] J. Peng, C. Roos, and T. Terlaky, *Self-Regularity: A New Paradigm for Primal-Dual Interior-Point Algorithms*. Princeton, NJ: Princeton University Press, 2002.

[30] M. R. Peyghami and S. Fathi-Hafshejani, "Complexity analysis of an interior-point algorithm for linear optimization based on a new proximity function," *Numerical Algorithms*, vol. 67, no. 1, pp. 33–48, 2014.

[31] M. R. Peyghami, S. Fathi-Hafshejani, and L. Shirvani, "Complexity of interior-point methods for linear optimization based on a new trigonometric kernel function," *Journal of Computational and Applied Mathematics*, vol. 255, pp. 74–85, 2014.

[32] J. Renegar, "A polynomial-time algorithm, based on Newton's method, for linear programming," *Mathematical Programming*, vol. 40, no. 1, pp. 59–93, 1988.

[33] C. Roos, T. Terlaky, and J.-P. Vial, *Theory and Algorithms for Linear Optimization: An Interior Point Approach*. Chichester, UK: John Wiley & Sons, 1997.

[34] B. Schweizer and A. Sklar, "Statistical metric spaces," *Pacific Journal of Mathematics*, vol. 10, no. 1, pp. 313–334, 1960.

[35] B. Schweizer and A. Sklar, *Probabilistic Metric Spaces*. New York: Elsevier Science Publishing, 1983.

[36] B. Schweizer, "Thirty years of copulas," in *Advances in Probability Distributions with Given Marginals*, G. Dall'Aglio, S. Kotz, and G. Salinetti, Eds., vol. 67. Dordrecht: Kluwer Academic Publishers, 1991.

[37] G. Wang and D. Zhu, "A unified kernel function approach to primal-dual interior-point algorithms for convex quadratic semidefinite optimization," *Numerical Algorithms*, vol. 57, no. 4, pp. 537–558, 2011.

[38] G. Q. Wang and Y. Q. Bai, "Primal-dual interior-point algorithm for convex quadratic semidefinite optimization," *Nonlinear Analysis: Theory, Methods & Applications*, vol. 71, nos. 7–8, pp. 3389–3402, 2009.

[39] S. J. Wright, *Primal-Dual Interior-Point Methods*. Philadelphia, PA: SIAM, 1997.

[40] S. Guerdouh, W. Chikouche, and I. Touil, "An efficient primal-dual interior point algorithm for linear optimization problems based on a novel parameterized kernel function with a hyperbolic barrier term," HAL preprint halshs-03228790, 2021.

[41] M. Li, M. Zhang, and Z. Huang, "A primal-dual interior-point method for linear optimization based on a new parameterized kernel function," *Journal of Nonlinear Functional Analysis*, vol. 2019, Article ID 38, 2019.

[42] Z. Moaberfard, S. Fathi-Hafshejani, and A. Fakharzadeh J., "An interior-point method for linear optimization based on a trigonometric kernel function," *Journal of Nonlinear Functional Analysis*, vol. 2019, Article ID 46, 2019.

[43] S. Fathi-Hafshejani and M. R. Peyghami, "An interior point algorithm for solving linear optimization problems using a new trigonometric kernel function," *Filomat*, vol. 34, no. 5, pp. 1471–1486, 2020.

[44] M. Bouafia and A. Yassine, "An efficient twice parameterized trigonometric kernel function for linear optimization," *Optimization and Engineering*, vol. 21, pp. 651–672, 2020.

[45] M. Bouafia and A. Yassine, "Complexity analysis of primal-dual interior-point methods for linear optimization based on a new efficient bi-parameterized kernel function with a trigonometric barrier term," *RAIRO-Operations Research*, vol. 56, pp. 731–750, 2022.

[46] L. Derbal and Z. Kebbiche, "Theoretical and numerical result for linear optimization problem based on a new kernel function," *Journal of Siberian Federal University. Mathematics & Physics*, vol. 12, no. 2, pp. 160–172, 2019.